Nanofabrication of Double-Gyroid Thin Films

Vikrant N. Urade,† Ta-Chen Wei,† Michael P. Tate,† Jonathan D. Kowalski, and Hugh W. Hillhouse*

School of Chemical Engineering, Purdue University, West Lafayette, Indiana 47907

Received September 8, 2006. Revised Manuscript Received November 27, 2006

Nanoporous silica films with the double-gyroid structure offer tremendous technological potential for sensors and separations because of their high surface area and potentially facile transport properties. Further, metals and semiconductors with similar structure open up new opportunities for high-surface-area electrodes, photoelectrochemical devices, photovoltaics, and thermoelectrics. Here, we report a new robust synthesis of highly ordered nanoporous silica films with the double-gyroid structure by evaporation-induced self-assembly (EISA) at room temperature and laboratory humidity using a commercially available $EO_{17}-PO_{12}-C_{14}$ surfactant. The continuous nanoporous films are synthesized on conducting electrodes. Electrochemical impedance spectroscopy is then used to quantitatively measure the accessible surface area of the underlying electrode via transport through the pore system. It is found that the double-gyroid-structure silica films expose a much higher fraction of the electrode than other commonly synthesized nanostructures such as 2D centered rectangular or 3D rhombohedral nanostructures. The double-gyroid nanoporous-film-coated electrodes are then used to fabricate inverse double-gyroid platinum nanostructures by electrodeposition, followed by etching to remove the silica. The structure of both the nanoporous silica films and the nanoporous platinum films (after etching) have been elucidated using high-resolution field-emission scanning electron microscopy (FESEM), comparing measured and simulated 2D grazing angle-of-incidence small-angle X-ray scattering (GISAXS) patterns, and comparing observed and simulated transmission electron microscopy (TEM) images. Both films are highly (211) oriented and described by a cubic $Ia\bar{3}d$ space group that has undergone uniaxial contraction perpendicular to the substrate. Upon this contraction, $Ia\bar{3}d$ symmetry is broken, but the films retain the double-gyroid topology. The nanoporous silica and the platinum nanowires have a characteristic wall or wire thicknesses of approximately 3 nm. This nanofabrication process opens up a facile general route for fabrication of ordered structures on the sub-5 nm length scale.

1. Introduction

Self-assembly is evolving as a key technology to fabricate nanoscale structures.[1,2] In particular, highly ordered nanoporous films that provide accessibility to an underlying substrate are a key cornerstone of nanofabrication. Synthesis routes based on both anodic oxidation of aluminum[3] and self-assembled block copolymers[4] have advanced rapidly and are now widely used to generate films with controlled pore sizes below 50 nm that directly access the substrate. The alignment of cylindrical microdomains of diblock copolymers under the influence of an electric field has been used to create 14 nm pores perpendicular to the substrate and Co and Pt nanowires have been electrodeposited in the pores.[5] However, for pore diameters smaller than 5 nm, similar milestones have not been reached, and there are no technologies that provide well-defined periodic access to a substrate at this length scale. This is an important size range, however, because surface area increases dramatically as pore size decreases (at constant void fraction) and many quantum size effects emerge only at these smaller length scales. As a result, developing such nanoporous films promises to enable the development of ultrasensitive high-surface-area sensors, high-surface-area electrodes for photoelectrochemical devices, and new nanostructured thermoelectrics and photovoltaics. In addition, films formed on macroporous substrates hold promise for size-selective separations.

The surfactant templating route, pioneered by scientists at Mobil,[6,7] can be used to generate ordered nanoporous metal oxides having a wide variety of structures[8−10] and compositions.[11−17] Evaporation-induced self-assembly (EISA) techniques can

* Corresponding author. E-mail: hugh@purdue.edu.
† These authors contributed equally to this work.

(1) Park, M.; Harrison, C.; Chaikin, P. M.; Register, R. A.; Adamson, D. H. *Science* **1997**, *276* (5317), 1401−1404.
(2) Lopes, W. A.; Jaeger, H. M. *Nature* **2001**, *414* (6865), 735−738.
(3) Masuda, H.; Fukuda, K. *Science* **1995**, *268* (5216), 1466−1468.
(4) Thurn-Albrecht, T.; Steiner, R.; DeRouchey, J.; Stafford, C. M.; Huang, E.; Bal, M.; Tuominen, M.; Hawker, C. J.; Russell, T. *Adv. Mater.* **2000**, *12* (11), 787−791.
(5) Thurn-Albrecht, T.; Schotter, J.; Kastle, C. A.; Emley, N.; Shibauchi, T.; Krusin-Elbaum, L.; Guarini, K.; Black, C. T.; Tuominen, M. T.; Russell, T. P. *Science* **2000**, *290* (5499), 2126−2129.
(6) Beck, J. S.; Vartuli, J. C.; Roth, W. J.; Leonowicz, M. E.; Kresge, C. T.; Schmitt, K. D.; Chu, C. T. W.; Olson, D. H.; Sheppard, E. W.; McCullen, S. B.; Higgins, J. B.; Schlenker, J. L. *J. Am. Chem. Soc.* **1992**, *114* (27), 10834−10843.
(7) Kresge, C. T.; Leonowicz, M. E.; Roth, W. J.; Vartuli, J. C.; Beck, J. S. *Nature* **1992**, *359* (6397), 710−712.
(8) Huo, Q. S.; Margolese, D. I.; Stucky, G. D. *Chem. Mater.* **1996**, *8* (5), 1147−1160.
(9) Zhao, D. Y.; Huo, Q. S.; Feng, J. L.; Chmelka, B. F.; Stucky, G. D. *J. Am. Chem. Soc.* **1998**, *120* (24), 6024−6036.
(10) Miyata, H.; Suzuki, T.; Fukuoka, A.; Sawada, T.; Watanabe, M.; Noma, T.; Takada, K.; Mukaide, T.; Kuroda, K. *Nat. Mater.* **2004**, *3* (9), 651−656.

10.1021/cm062136n CCC: $37.00
Published on Web 01/18/2007

be used to synthesize ordered nanoporous materials in thin film and monolith form.[18−20] Further, electrochemical deposition in such ordered nanoporous materials can be used to generate new materials for the devices mentioned above. However, this method requires that solution-phase species are able to access an underlying electrode through the pore system and transfer electrons across the interface. One way to generate this access is to self-assemble a highly ordered 3D nanoporous film based on the gyroid minimum surface[21] (which has $Ia\bar{3}d$ symmetry and is referred to as the G-surface). This zero mean curvature surface divides space into two continuous, non-intersecting domains. The nomenclature used to describe physical structures based on the G-surface varies in the literature, so we clarify our terms here. When a finite-thickness wall replaces the G-surface, a tricontinuous structure results (with the silica wall and two pore systems constituting the three continuous systems). Here, we refer to this nanostructure as the double-gyroid structure to indicate that the silica wall is enclosed between two surfaces that can be obtained by displacing the gyroid surface by half the silica wall thickness in the positive and negative directions. This same structure has been referred to by some previous authors as "bicontinuous." However, this may be confusing, because there are two-component structures where component 1 lies on one side of G-surface and component 2 lies on the other side. Such materials are truly bicontinuous and have $I4_132$ symmetry,[22] not $Ia\bar{3}d$ symmetry, as the tricontinuous structure and the G-surface itself. We use the term "inverse double-gyroid" here to indicate a material formed by filling the pores of a nanoporous double-gyroid structure followed by removal of the original material that was centered on the G-surface. In the inverse double-gyroid structure, the G-surface defines the location of the pore, which is centered on the G-surface.

Double-gyroid structures have been observed in block copolymer systems and typically occur between the lamellar and cylindrical phases on the spectrum of interfacial curvature.[23−30] In addition, topologies based on other minimal surfaces (such as the P-type "plumber's nightmare" surface with $Im\bar{3}m$ symmetry) have been observed in millimeter-thick films of block−copolymer/ceramic nanocomposites.[31] However, the first double-gyroid structured nanoporous silica was synthesized in particulate morphology using ionic surfactants and silica oligomers.[7] Since this first report, many techniques have been developed to tune interfacial curvature to make mesoporous double-gyroid structure powders, including the use of swelling agents and cosurfactant.[32] However, it is difficult to adapt these methods used in powder synthesis to tune the interfacial curvature of the silica−surfactant interface during film synthesis by evaporation-induced self-assembly. To control the quantity of an additive in the film during evaporation, one needs to control its chemical potential in the vapor phase. Because of this requirement and the narrow range of interfacial curvature where the gyroid phase usually exists, there are only two reports of synthesis of nanoporous silica films with gyroid-based structures. In the first report, large-pore, double-gyroid films were synthesized using custom-made silicon-containing triblock copolymers.[33] Later, a synthesis was developed using Brij surfactants along with a post-coating thermal treatment at elevated temperatures to obtain gyroid films.[34] However, the double-gyroid structure is obtained over a very narrow temperature range and multiphase films are often obtained.

Here, we report a new method for simple and robust room-temperature self-assembly of double-gyroid nanostructured silica films from commercially available poly(ethylene oxide)-poly(propylene oxide)-alkane surfactants, quantitative electrochemical measurements of species accessibility to the substrate through the nanopore structure, and the use of these films in a general route for the fabrication of stable double-gyroid nanostructured metal films. To the best of the authors' knowledge, this is the first report of quantitatively accurate measurements of the accessibility of solution-phase species to the substrate through self-assembled nanoporous silica

(11) Grosso, D.; Boissiere, C.; Smarsly, B.; Brezesinski, T.; Pinna, N.; Albouy, P. A.; Amenitsch, H.; Antonietti, M.; Sanchez, C. *Nat. Mater.* **2004**, *3* (11), 787−792.
(12) Angelome, P. C.; Aldabe-Bilmes, S.; Calvo, M. E.; Crepaldi, E. L.; Grosso, D.; Sanchez, C.; Soler-Illia, G. *New J. Chem.* **2005**, *29* (1), 59−63.
(13) Brezesinski, T.; Smarsly, B.; Groenewolt, M.; Antonietti, M.; Grosso, D.; Boissiere, C.; Sanchez, C. The generation of mesoporous CeO_2 with crystalline pore walls using novel block copolymer templates. In *Nanoporous Materials IV*; Proceedings of the 4th International Symposium on Nanoporous Materials, Niagra Falls, ON, June 7−10, 2005; Sayari, A., Jaroniec, M., Eds.; Elsevier: Amsterdam, 2005; Vol. 156, pp 243−248.
(14) Brezesinski, T.; Smarsly, B.; Iimura, K.; Grosso, D.; Boissiere, C.; Amenitsch, H.; Antonietti, M.; Sanchez, C. *Small* **2005**, *1* (8−9), 889−898.
(15) de Zarate, D. O.; Boissiere, C.; Grosso, D.; Albouy, P. A.; Amenitsch, H.; Amoros, P.; Sanchez, C. *New J. Chem.* **2005**, *29* (1), 141−144.
(16) Kuemmel, M.; Grosso, D.; Boissiere, U.; Smarsly, B.; Brezesinski, T.; Albouy, P. A.; Amenitsch, H.; Sanchez, C. *Angew. Chem., Int. Ed.* **2005**, *44* (29), 4589−4592.
(17) Shi, K. Y.; Peng, L. M.; Chen, Q.; Wang, R. H.; Zhou, W. Z. *Microporous Mesoporous Mater.* **2005**, *83* (1−3), 219−224.
(18) Ogawa, M. *Chem. Commun.* **1996**, 1149−1150.
(19) Ogawa, M.; Ishikawa, H.; Kikuchi, T. *J. Mater. Chem.* **1998**, *8* (8), 1783−1786.
(20) Brinker, C. J.; Lu, Y. F.; Sellinger, A.; Fan, H. Y. *Adv. Mater.* **1999**, *11* (7), 579.
(21) Schoen, A. H. *Infinite Periodic Minimal Surfaces without Self-Intersections*; NASA Technical Note #D5541; NASA: Washington, D.C., 1970.
(22) Garstecki, P.; Holyst, R. *Macromolecules* **2003**, *36* (24), 9181−9190.
(23) Luzzati, V.; Spegt, P. A. *Nature* **1967**, *215* (5102), 701−704.
(24) Luzzati, V.; Tardieu, A.; Gulik-Krzywicki, T.; Rivas, E.; Reiss-Husson, F. *Nature* **1968**, *220* (5166), 485−488.
(25) Hyde, S. T.; Andersson, S.; Ericsson, B.; Larsson, K. *Z. Kristallogr.* **1984**, *168* (1−4), 213−219.
(26) Hajduk, D. A.; Harper, P. E.; Gruner, S. M.; Honeker, C. C.; Kim, G.; Thomas, E. L.; Fetters, L. J. *Macromolecules* **1994**, *27* (15), 4063−4075.
(27) Bates, F. S.; Fredrickson, G. H. *Phys. Today* **1999**, *52* (2), 32−38.
(28) Dair, B. J.; Honeker, C. C.; Alward, D. B.; Avgeropoulos, A.; Hadjichristidis, N.; Fetters, L. J.; Capel, M.; Thomas, E. L. *Macromolecules* **1999**, *32* (24), 8145−8152.
(29) Hamley, I. W.; Fairclough, J. P. A.; Ryan, A. J.; Mai, S. M.; Booth, C. *Phys. Chem. Chem. Phys.* **1999**, *1* (9), 2097−2101.
(30) Sakurai, S.; Isobe, D.; Okamoto, S.; Yao, T.; Nomura, S. *Phys. Rev. E* **2001**, *63* (6).
(31) Finnefrock, A. C.; Ulrich, R.; Toombes, G. E. S.; Gruner, S. M.; Wiesner, U. *J. Am. Chem. Soc.* **2003**, *125* (43), 13084−13093.
(32) Kim, T. W.; Kleitz, F.; Paul, B.; Ryoo, R. *J. Am. Chem. Soc.* **2005**, *127* (20), 7601−7610.
(33) Chan, V. Z. H.; Hoffman, J.; Lee, V. Y.; Iatrou, H.; Avgeropoulos, A.; Hadjichristidis, N.; Miller, R. D.; Thomas, E. L. *Science* **1999**, *286* (5445), 1716−1719.
(34) Hayward, R. C.; Alberius, P. C. A.; Kramer, E. J.; Chmelka, B. F. *Langmuir* **2004**, *20* (14), 5998−6004.

films and the first report of inverse double-gyroid metal nanostructured films that retain both long-range and short-range order after removal of the original template.

2. Experimental Section

2.1. Synthesis of Nanoporous Silica Films. The surfactant with the nominal chemical structure $H(CH_2CH_2O)_{17}$-$(CH(CH_3)CH_2O)_{12}$-$C_{14}H_{29}$ (hereinafter referred to as $EO_{17}-PO_{12}-C_{14}$) was a gift from Dow Chemicals and was used as received. Tetraethyl orthosilicate (TEOS, 98% w/w, obtained from Aldrich) was used as silica source. Hydrochloric acid (37% w/w) was from Aldrich and ethyl alcohol from EMD Chemicals (>99.5% v/v). All chemicals were ACS reagent grade and were used as-received. For double-gyroid silica films, TEOS was prehydrolyzed at room temperature (21 °C). A solution of 6.35 g of HCl in water at pH 1.76 was added to 12.86 g of ethanol in an HDPE bottle. TEOS (12.2 g) was then added quickly. The bottle was immediately sealed and stirred for 20 min at 21 °C. The prehydrolysis solution had a 1:0.0019:6.0:4.8 TEOS:HCl:H_2O:EtOH molar ratio. Immediately after prehydrolysis, 13.9 g of a 37 wt % solution of $EO_{17}-PO_{12}-C_{14}$ in ethanol (equilibrated for 12 h) was added to form the coating solution. The coating solution was then aged for different times at 21 °C. The final molar composition of the coating solution was 1:0.054:0.0019:6.0:8.0 TEOS:$EO_{17}-PO_{12}-C_{14}$:HCl:H_2O:EtOH. Before coating, fluorine-doped SnO_2 (FTO) substrates were cleaned by immersion in 1 wt % Alconox at 65 °C for 30 s followed by being rinsed with copious quantities of RO water and air-dried. Films were dip-coated on FTO using this solution at a withdrawal speed of 1 mm/s. High-quality films were formed after being dip-coated at 40% relative humidity (RH) after 10 days of aging of the coating solution. After coating, films were left at the same RH for 12 h and then calcined in air at 400 °C for 4 h (with 1 °C/min ramps). Contracted 2D hexagonal films (plane group *c*2*m*) were synthesized as published by Cagnol,[35] and contracted face-centered cubic films (rhombohedral space group $R\bar{3}m$) were synthesized as published previously.[36]

2.2. Grazing Angle-of-Incidence Small-Angle X-ray Scattering (GISAXS) Characterization. The GISAXS setup consists of a standard three-pinhole camera (Molecular Metrology) with a Bede microfocus Cu$-K_\alpha$ X-ray source ($\lambda = 1.54$ Å) and Osmic MaxFlux graded multilayer optics. The patterns are collected on a 12.5 cm diameter 2D multiwire gas-filled detector. The detector was calibrated using silver behenate standard. The schematic of the setup is shown in Figure 1. The GISAXS patterns were calculated using a *Mathematica*-based program called NANOCELL[37] and overlaid on the actual patterns. The lattice constants were varied until a good match was seen between the peak positions in the observed and actual patterns. The variables α_i, α_f, and $2\theta_f$ used in the overlays in GISAXS patterns are explained in Figure 1.

2.3. Determination of Accessible Area of the Substrate. A standard three-electrode cell was used for all experiments with the calcined nanoporous film coated FTO as the working electrode (1.5 cm^2 geometric area submersed), a platinum wire with an active area of 20 cm^2 as the counter electrode, and Ag/AgCl in saturated KCl as the reference electrode. The electrolyte contained 1 mM 1,1′-ferrocenedimethanol redox couple, 1 M KCl as supporting electrolyte, and 0.01 M HCl such that the pH of the solution was close to 2. The formal potential was determined to be 0.21 V (vs Ag/AgCl) by cyclic voltammetry using PAR 283 potentiostat. Electrochemical impedance spectroscopy (EIS) data were then collected using a Solartron 1260 frequency response analyzer with a DC bias set to the measured formal potential, superimposed on which was an AC bias of magnitude 10 mV (rms). These data were collected over a frequency range from 0.1 Hz to 100 kHz. The complex and real part of the impedance were plotted parametrically with frequency (an Argand diagram) and were made to fit desired equivalent circuit models using complex nonlinear least-squares fitting. A Randles equivalent circuit provided a good fit for the bare electrode data. For nanoporous-film-coated electrodes, a modified Randles circuit with a constant phase element (CPE) substituting the double-layer capacitance and a Warburg element were used. The accessible area was then calculated from the charge-transfer resistance for the one-electron reaction given by $R_{ct} = RT/F^2kAPC$, where k is the standard rate constant, A the accessible substrate area, P the partition coefficient of the redox couple in the film, C the bulk concentration of the redox couple, and F the Faraday constant. k was determined by EIS on a bare electrode under identical conditions. In the absence of a specific interaction between the redox couple and the silica wall and for pores much larger than the redox couple, P will approach unity. At pH 2 (where all EIS data were collected in this study), the silica wall is neutral and decorated with hydroxyl groups. As such, the partition coefficient is expected to be very close to unity. Further, at pH values close to 2, hydrolytic degradation of the silica film is negligible, as EIS experiments on the same film immersed for several days in the solution yield the same value of the measured accessible area.

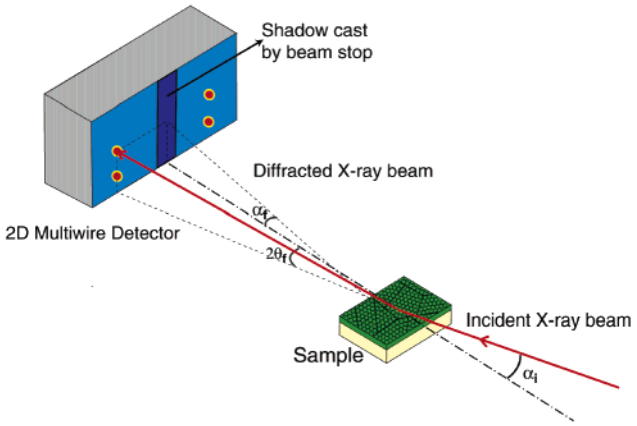

Figure 1. Setup used for grazing incidence small-angle X-ray scattering (GISAXS) data collection. The nanoporous thin film, sampling multiple orientations about a direction normal to the substrate, gives patterns that are symmetrical about the vertical axis on the detector. This schematic illustrates the variables α_i, α_f, and $2\theta_f$ used in the overlays in GISAXS patterns.

2.4. Nanofabrication by Electrodeposition in Nanoporous Silica Films. The same three-electrode cell described above was used for potentiostatic depositions. The working electrode (nanoporous film coated FTO) was immersed in a deoxygenated electrolyte solution for 10 min prior to deposition. Here, we describe the procedure used to prepare platinum nanowire arrays as a representative example of the electrodeposition route that can be generalized to other metals and semiconductor systems. The electrolyte used for Pt deposition was 0.022 M hexachloroplatinic acid (H_2PtCl_6) in deionized water (pH 1.5). The depositions were carried out at a constant potential of −0.3 V vs Ag/AgCl at 21 °C until the current integrated to 0.4 C/cm^2. The silica was then removed by etching the film in a 2 wt % HF solution for 4 h at 21 °C.

(35) Cagnol, F.; Grosso, D.; Soler-Illia, G.; Crepaldi, E. L.; Babonneau, F.; Amenitsch, H.; Sanchez, C. *J. Mater. Chem.* **2003**, *13* (1), 61−66.
(36) Eggiman, B. W.; Tate, M. P.; Hillhouse, H. W. *Chem. Mater.* **2006**, *18* (3), 723−730.
(37) Tate, M. P.; Urade, V. N.; Kowalski, J. D.; Wei, T. C.; Hamilton, B. D.; Eggiman, B. W.; Hillhouse, H. W. *J. Phys. Chem. B* **2006**, *110* (20), 9882−9892.

3. Results and Discussion

3.1. Robust Synthesis of Double-Gyroid Structure Nanoporous Silica Films. For EISA of nanoporous silica films, the coating solution contains silica species that undergo condensation reactions and evolve with aging time prior to dip-coating/spin-coating and solvent evaporation. As a result, there is typically a window of time over which EISA yields an ordered nanostructure[38] that depends on the pH and hydrolysis ratio.[39] In addition, the vapor-phase composition (humidity) plays a key role in determining the interfacial curvature of the nanostructure.[35] These aspects and other key factors were recently elaborated in a thorough review and analysis of EISA of nanostructured thin films,[40] focusing on CTAB-templated films. Our results with CTAB as the structure-directing agent indicate that the aging time primarily affects the degree of order of the nanostructure in CTAB−silica system, not the type of nanostructure obtained. However, we find here that for films templated by surfactants containing polyethylene oxide (PEO) as the hydrophilic component, aging of the coating solution provides a means to precisely and robustly control the interfacial curvature and thus the phase that self-assembles. Details of this phenomena and a discussion of the mechanism will follow in future publication.

We used this controlled aging time approach to synthesize nanoporous films with the double-gyroid structure using an $EO_{17}-PO_{12}-C_{14}$ copolymer. After mixing the coating solution, films formed by EISA show a systematic progression from high to low curvature silica nanostructures with increasing aging time. After 10 days of aging at room temperature, high-quality pure double-gyroid phase nanostructured films self-assemble when dip-coated at 40% relative humidity (Figure 2). The time window where good quality films may be dip-coated extends up to 15 days when the coating solution is stored at room temperature. However, if the coating solution is refrigerated after 10 days of aging at room temperature, consistently high-quality nanoporous silica films with the double-gyroid structure are obtained even after 3 months of storage and even when dip-coated over a broader range of relative humidity (ca. 40−70%). An upper limit to the aging time (under refrigeration) has not yet been established.

3.2. Film Structure, Order, and Orientation. Grazing angle-of-incidence small-angle X-ray scattering (GISAXS) was used to determine the symmetry, order, and orientation of the films. The GISAXS patterns were interpreted using the distorted wave born approximation (DWBA) to include the effects of refraction and reflection[37] at the film−substrate and film−air interfaces and calculate the positions of the Bragg diffraction spots (Figure 3). It was found that the Bragg spots of the as-synthesized film can be accurately described by cubic structure that is highly oriented with its

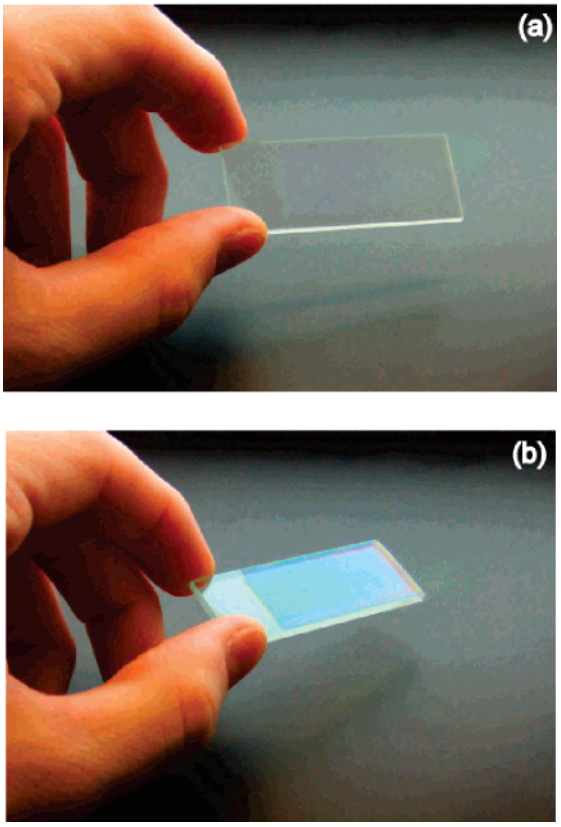

Figure 2. Photographs of a double-gyroid-phase nanoporous silica film on a fluorine-doped tin oxide substrate. (a) Transparency and optical perfection of the film. (b) Film tilted slightly, whereupon an iridescent blue interference color is observed due to the ca. 350 nm thickness of the film. The uniformity of the color indicates the uniformity of thickness and perfection of the film.

(211) planes parallel to the substrate and has undergone a 7% contraction perpendicular to the substrate. The lattice constants for the unidirectionally contracted structure were determined as follows. First, it is noted that the positions of peaks along the $\alpha_f = 0°$ axis (which correspond to spacings between planes perpendicular to the substrate) ideally do not change when the unit cell is compressed along a direction perpendicular to the substrate, whereas the peaks along the $2\theta_f = 0°$ axis directly reflect any contraction. Thus, the peaks along the $\alpha_f = 0°$ axis allow one to estimate the one independent lattice constant (a) for the initial uncontracted ($\alpha = \beta = \gamma = 90°$) cubic structure. Next, we note that there should be only four unique lattice constants for the unidirectionally contracted (211) oriented cubic structure upon a compression perpendicular to the (211) direction, because $b = c$ and $\beta = \gamma$. However, these four lattice constants are related to the extent of the unidirectional contraction. Thus, there are only two independent parameters to simulate the diffraction patterns: the lattice constant a of initial true gyroid structure and the extent of unidirectional contraction. The extent of unidirectional contraction is adjusted until the calculated peak positions match the observed positions by visual comparison. Using this technique, it was determined that the as-synthesized structure contracted by 7% whereas the calcined structure contracted by 40%.

Despite the fact that the as-synthesized films undergo a unidirectional contraction upon drying, the systematic extinctions in the pattern were perfectly described by $Ia\bar{3}d$

(38) Klotz, M.; Ayral, A.; Guizard, C.; Cot, L. *J. Mater. Chem.* **2000**, *10* (3), 663−669.
(39) Grosso, D.; Babonneau, F.; Albouy, P. A.; Amenitsch, H.; Balkenende, A. R.; Brunet-Bruneau, A.; Rivory, J. *Chem. Mater.* **2002**, *14* (2), 931−939.
(40) Grosso, D.; Cagnol, F.; Soler-Illia, G.; Crepaldi, E. L.; Amenitsch, H.; Brunet-Bruneau, A.; Bourgeois, A.; Sanchez, C. *Adv. Funct. Mater.* **2004**, *14* (4), 309−322.

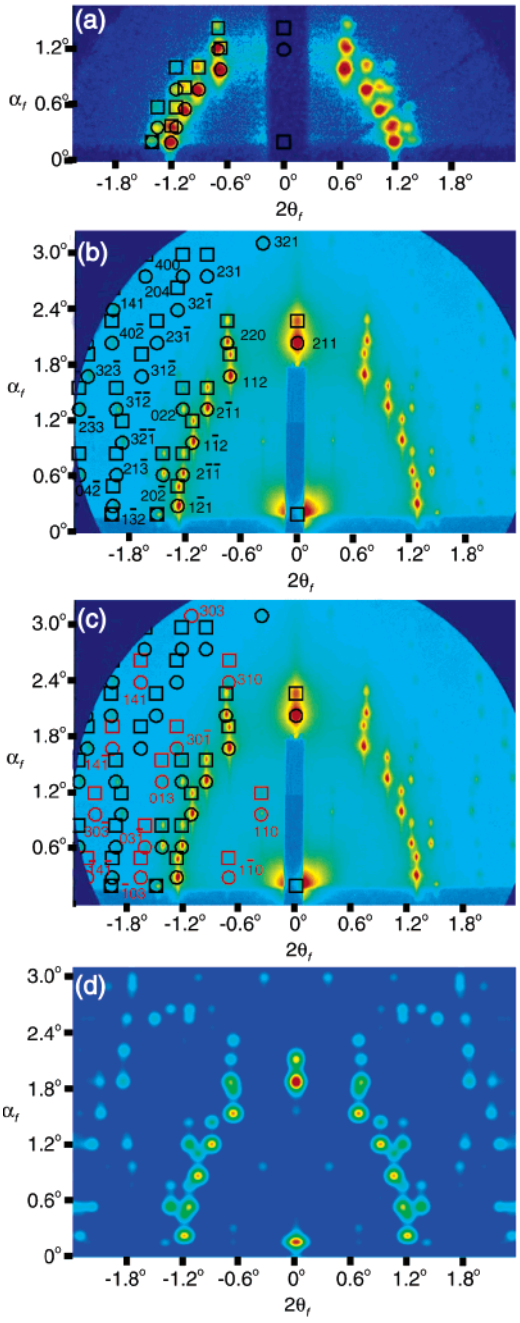

Figure 3. GISAXS patterns of the nanostructured tricontinuous films before and after template removal. Data were collected at an angle-of-incidence of 0.2°, just above the critical angle, from films on fluorine-doped tin oxide (FTO) substrates. The scattering patterns are symmetric about $2\theta_f = 0°$. For clarity, the experimental data is overlaid with the predicted diffraction spot positions on only one side of the pattern so that the intensity of the spots can clearly be seen on the other side. The positions are calculated under the DWBA using NANOCELL.[37] The circles indicate diffraction from the refracted incident beam, whereas the squares indicate diffraction from the refracted and reflected incident beam. (a) CuK_α GISAXS of as-synthesized film with an overlay of predicted positions from a (211) oriented unit cell with $a = 17.1$ nm, $b = 17.6$ nm, $c = 17.6$ nm, $\alpha = 91.1°$, $\beta = 92.3°$, $\gamma = 92.3°$, possessing all the double-gyroid extinction conditions. (b) Synchrotron GISAXS pattern of a nanoporous silica film after template removal by calcination with an overlay with $a = 13.5$ nm, $b = 16.8$ nm, $c = 16.8$ nm, $\alpha = 97°$, $\beta = 107°$, $\gamma = 107°$. Note that all high-intensity peaks are still described using the double-gyroid extinction conditions. However, some weaker peaks appear when compared to (a). (c) Same data as in part b, with an overlay that includes peaks arising from broken glide-plane symmetry elements (shown in red). (d) Simulation of the scattering intensity from a nanoporous double-gyroid film (as seen in Figure 10a) using the DWBA and a discrete Fourier transform of the electron density described by eq 1.

symmetry (Figure 3a). In principle, $Ia\bar{3}d$ symmetry must be broken, but as noted previously by Garsteki and Holyst,[22] the exact shape of the surface does not significantly effect the X-ray diffraction pattern. This good agreement with $Ia\bar{3}d$ extinction conditions allows us to diagnose the structure as tricontinuous as opposed to bicontinuous. The "bicontinuous" $I4_132$ structure has high relative intensity peaks that are not observed in the as-synthesized films. Amazingly, the main features of the GISAXS pattern are still preserved in the calcined nanoporous film, which has undergone a 40% contraction perpendicular to the substrate. However, at these very large values of unidirectional contraction, some low-intensity peaks not belonging to the $Ia\bar{3}d$ symmetry do appear. These can be used to identify which symmetry elements are most severely broken. These broken symmetries are *b* and *c* glide planes parallel to the (100) of the uncontracted cubic structure; the *c* and *a* glide planes parallel to the (010); the *d* glide planes parallel to the $(1\bar{1}0)$ and (110); and the *d* glide planes parallel to the $(\bar{1}01)$ and (101). These relax the extinction conditions $0kl$ (for $k,l = 2n$); $h0l$ (for $h,l = 2n$); hhl and $h\bar{h}l$ (for $2h + l = 4n$); and hkh and $-hkh$ (for $2h+k = 4n$), respectively. Thus, the GISAXS data also suggests that the nanoporous silica film has the double-gyroid structure with the silica wall lying on the G-surface.

The structure and topology of the nanoporous silica films were also examined by transmission electron microscopy (TEM) (Figure 4) and field-emission scanning electron microscopy (FESEM) imaging (Figure 5). Experimental TEM images were compared with projections of electron density calculated from several possible structures that are based on the gyroid minimum surface. An excellent match was found between the observed TEM images and those simulated only from a tricontinuous structure where the gyroid minimal surface runs down the center of a silica wall separating the two pore systems. The uncontracted cubic structure was modeled using the level surface approximation for a double gyroid phase,[41] derived here in terms of electron density $\rho(x,y,z)$ and the wall thickness (w) as

$$\rho(x,y,z) = \begin{cases} 1 \text{ for } \left|\sin\left(\frac{2\pi x}{a}\right)\cos\left(\frac{2\pi y}{a}\right) + \sin\left(\frac{2\pi y}{a}\right)\cos\left(\frac{2\pi z}{a}\right) + \sin\left(\frac{2\pi z}{a}\right)\cos\left(\frac{2\pi x}{a}\right)\right| \le \sqrt{2}\sin\left(\frac{\pi w}{a}\right) \\ 0 \text{ otherwise} \end{cases} \quad (1)$$

where a is the lattice constant of the uncontracted cubic structure (determined from GISAXS of planes perpendicular to the substrate to be 17.9 nm). The right-hand side gives the absolute value of the contour of the level surface in terms of the wall thickness (w) at the 24d Wyckoff position (space group $Ia\bar{3}d$). The structure defined by this equation was then oriented such that the (211) planes were parallel to the substrate and then uniaxially contracted by 40% toward the substrate (by applying rotation and deformation matrices). The projected electron densities along any given [*hkl*] direction were then calculated by integration and compared

(41) Wohlgemuth, M.; Yufa, N.; Hoffman, J.; Thomas, L. E. *Macromolecules* **2001**, *34*, 6083−6089.

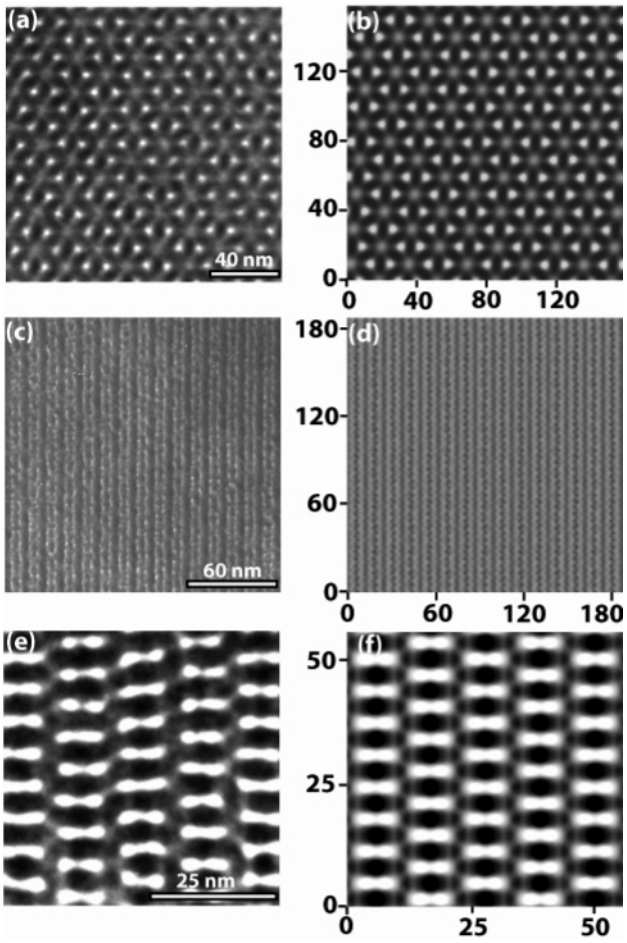

Figure 4. Transmission electron microscopy images for the double-gyroid silica films calcined at 400 °C. Observed TEM images and simulated electron density projections are shown for the (a, b) [111], (c, d) [211], and (e, f) [311] projections. The axes in parts b, d, and f are in units of nanometers and show simulations for a contour value of 1.1 with 40% contraction. Observed TEM images were obtained at 200 kV from nanoporous film fragments scraped from FTO substrates. As a result, the [111] and [311] projections were obtained at the edges of fragments and were thus relatively thin. However, the [211] projections are by far the dominant observed projection and are imaged through the thickness of the film fragments.

to observed TEM images. A Gaussian blur was applied to the projected density to account for aberration in the imaging process.

Here, it should be noted that the electron density projections should only be identical to simulated TEM images for an electron beam that is perfectly coherent and for a sample that is extremely thin. Despite this, the simple electron density projections compare extremely well to the observed TEM images and confirm the tricontinuous topology of the nanostructure. The best match between observed and simulated TEM images was obtained at a contour value of 1.1, corresponding to a silica wall thickness of ~5 nm at the 24d Wyckoff position prior to applying rotation matrices and contraction. It was recently suggested[42] on the basis of high-resolution TEM and electron crystallography of gyroid structure nanoporous silica powders that the silica wall may be thinner at the 16a Wyckoff position than other locations.

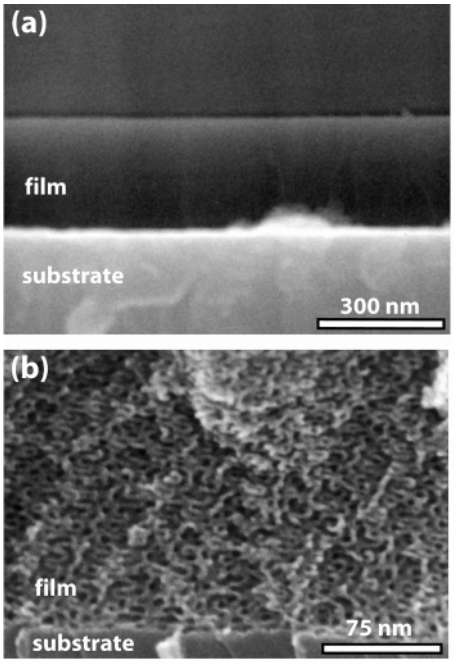

Figure 5. FESEM images of double-gyroid silica films calcined at 400 °C. (a) Low-magnification cross-sectional image of the film showing a typical film thickness of about 300 nm. (b) Highly ordered double-gyroid-derived nanostructure seen in the high-magnification FESEM image.

However, the resolution of the reconstruction reported here is too low to determine if similar structural phenomena occur in these films.

3.3. Electrochemically Accessible Area of the Substrate. The accessibility of pore volume in nanoporous powders is typically determined using nitrogen adsorption. However, this technique is not capable of giving any direct indication of accessibility to the substrate underlying a nanoporous film. Also, because of solvation and surface charge effects, the accessibility of the substrate to solution-phase species can be vastly different from the accessibility of gas-phase species. Electrochemical techniques may be used to address this question, but care must be taken to calculate accurate values of the accessible area. There have been only a few electrochemical studies that involve self-assembled continuous nanoporous film coated electrodes.[43−46] However, only one reports a quantitative measure of the accessible substrate area.[46] By comparing the peak currents from cyclic voltammetry (CV) of coated and bare electrodes, the authors conclude that 70% of the substrate is electrochemically accessible. However, this method is accurate only when the diffusion layer thickness (δ) is much smaller than the length scale of active regions of the electrode (d_a) where the electrochemical reactions occur and the distance of separation between the active regions (d_s). However, when $\delta \gg d_a$ and $\delta \gg d_s$, as is the case for surfactant-templated nanoporous

(42) Sakamoto, Y.; Kim, T. W.; Ryoo, R.; Terasaki, O. *Angew. Chem., Int. Ed.* **2004**, *43* (39), 5231−5234.

(43) Song, C. J.; Villemure, G. *Microporous Mesoporous Mater.* **2001**, *44*, 679−689.

(44) Liu, N. G.; Dunphy, D. R.; Atanassov, P.; Bunge, S. D.; Chen, Z.; Lopez, G. P.; Boyle, T. J.; Brinker, C. J. *Nano Lett.* **2004**, *4* (4), 551−554.

(45) Etienne, M.; Walcarius, A. *Electrochem. Commun.* **2005**, *7* (12), 1449−1456.

(46) Rohlfing, D. F.; Rathousky, J.; Rohlfing, Y.; Bartels, O.; Wark, M. *Langmuir* **2005**, *21* (24), 11320−11329.

films, this method may greatly overestimate of the accessible surface area.[47]

In general, CV and chronoamperometry present difficulties in determining the accessible substrate area because of their dependence on diffusion. However, electrochemical impedance spectroscopy (EIS) can be used to separate the effects of diffusion, solution resistance, and double-layer charging from the interfacial kinetics. This method has been used to great advantage to examine the fractional surface coverage of self-assembled monolayers.[48,49] In this method, a small magnitude sinusoidal voltage, $V(\omega)$, is superimposed on the applied DC potential, set to the formal potential of the redox couple. Because the applied DC bias is equal to the formal potential, we expect the concentrations of the oxidized and reduced forms to be equal in the film. The current response, $I(\omega)$, is measured and the complex impedance is calculated via $Z(\omega) = V(\omega)/I(\omega)$ over a broad range of frequencies. If the impedance data can be fit to simple, physically reasonable, equivalent circuits, then the accessible area of a bare or monolayer-coated substrate may be accurately determined from the charge-transfer resistance. For an electrode coated with a nanoporous film, only the product of the accessible area (A) and the partition coefficient (P) may be determined unambiguously. In the absence of a specific interaction between the redox couple and the silica wall and for pores much larger than the redox couple, P will approach unity. At pH 2 (where all EIS data were collected in this study), the silica wall is neutral and decorated with hydroxyl groups. As such, the partition coefficient is expected to be very close to unity. Further, at pH 2, hydrolytic degradation of the silica film is negligible, as EIS experiments on the same film immersed for days in the solution yield the same value of the measured accessible area.

The EIS data of ferrocene dimethanol on a bare FTO electrode fit a Randles equivalent circuit.[50] The charge-transfer resistance yielded a value of the standard rate constant of 0.0045 cm/s (using the geometric area of the bare FTO). The measured real and imaginary components of the electrochemical impedance and fitted equivalent circuit models are shown in Figure 6 as parametric plots as a function of frequency. FTO electrodes coated with crack-free nanoporous silica films show a slightly depressed semicircle in their impedance spectra. This is due to the fact that the double layer at the electrode surface is not a simple planar surface, but extends slightly into the wall structure of the film. Replacing the double layer capacitance (C_{dl}) with a constant phase element (CPE) allows one to model this deviation from planarity.[51] The impedance due to a CPE is given by $Z_{CPE} = 1/T(j\omega)^p$. The fractional exponent p characterizes the width of the relaxation time distribution due to the inhomogeneity, and $p = 1$ represents a single pure

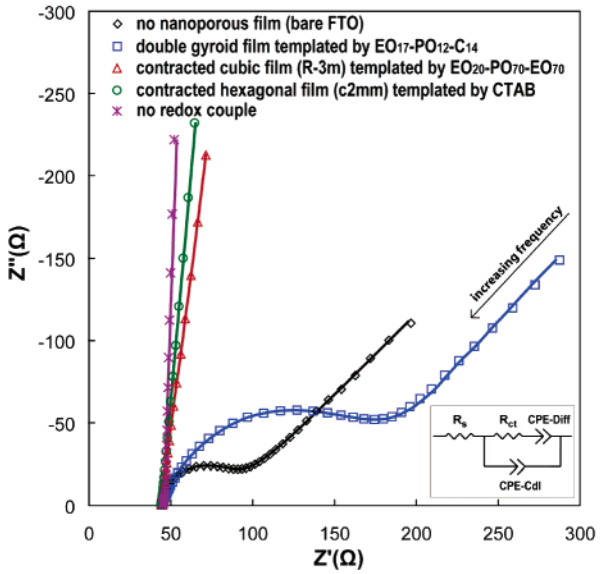

Figure 6. Electrochemical impedance spectroscopy (EIS) data plotted parametrically with frequency. The observed data (symbols) were fitted by an equivalent circuit (solid line), shown in the inset. The equivalent circuit element R_s is the same for all measurements and is primarily due to to the sheet resistance of the FTO substrate.

capacitor. The behavior of the diffusion impedance in the mass-transfer-controlled regime (low frequency) deviates slightly from that expected from Fickian 1D diffusion (an infinite-length Warburg element or a CPE with $p = 0.5$). A CPE is used to model this data and yielded a value of $p = 0.59$. However, this element does not affect the value of R_{ct}, which is dictated by the higher frequency data where the diffusion impedance is very small.

EIS data were collected from many topologies of nanoporous silica films and reveal that highly ordered and oriented contracted 2D hexagonal films and contracted 3D cubic films (synthesized using both $EO_{20}-PO_{70}-EO_{20}$[36] and $EO_{17}-PO_{12}-C_{14}$ and having rhombohedral space group $R\bar{3}m$) have extremely low accessible substrate areas (less than 0.02%) for the ~6 Å diameter ferrocene dimethanol probe molecule. However, the new double-gyroid films synthesized here have accessible areas of 31 ± 3% (Figure 6). All surface areas have been calculated assuming a partition coefficient of 1. The low accessibility in 2D hexagonal films is expected, because the mesopores are aligned parallel to the substrate. However, low accessibility in rhombohedral films is surprising, as these films show large nanopore openings in top-view FESEM[52] and are expected to have intercage connections similar to those observed in cubic phase nanoporous silica powders,[53] particularly $Fm3m$ structures.[54] This lack of accessibility in highly ordered rhombohedral films could be due to the lack of intercage openings or the presence of a thin but dense silica layer beneath the nanoporous region. The accessibility increases for hexagonal and rhombohedral

(47) Amatore, C.; Saveant, J. M.; Tessier, D. *J. Electroanal. Chem.* **1983**, *147* (1−2), 39−51.
(48) Sabatani, E.; Cohenboulakia, J.; Bruening, M.; Rubinstein, I. *Langmuir* **1993**, *9* (11), 2974−2981.
(49) Janek, R. P.; Fawcett, W. R.; Ulman, A. *Langmuir* **1998**, *14* (11), 3011−3018.
(50) Bard, A. J.; Faulkner, L. R. *Electrochemical Methods: Fundamentals and Applications*; Wiley: New York, 2001.
(51) Macdonald, J. R.; Barsoukov, E. *Impedance Spectroscopy: Theory, Experiment, and Applications*; Wiley-Interscience: Hoboken, NJ, 2005.
(52) Tate, M. P.; Eggiman, B. W.; Kowalski, J. D.; Hillhouse, H. W. *Langmuir* **2005**, *21* (22), 10112−10118.
(53) Sakamoto, Y.; Kaneda, M.; Terasaki, O.; Zhao, D. Y.; Kim, J. M.; Stucky, G.; Shim, H. J.; Ryoo, R. *Nature* **2000**, *408* (6811), 449−453.
(54) Kleitz, F.; Liu, D. N.; Anilkumar, G. M.; Park, I. S.; Solovyov, L. A.; Shmakov, A. N.; Ryoo, R. *J. Phys. Chem. B* **2003**, *107* (51), 14296−14300.

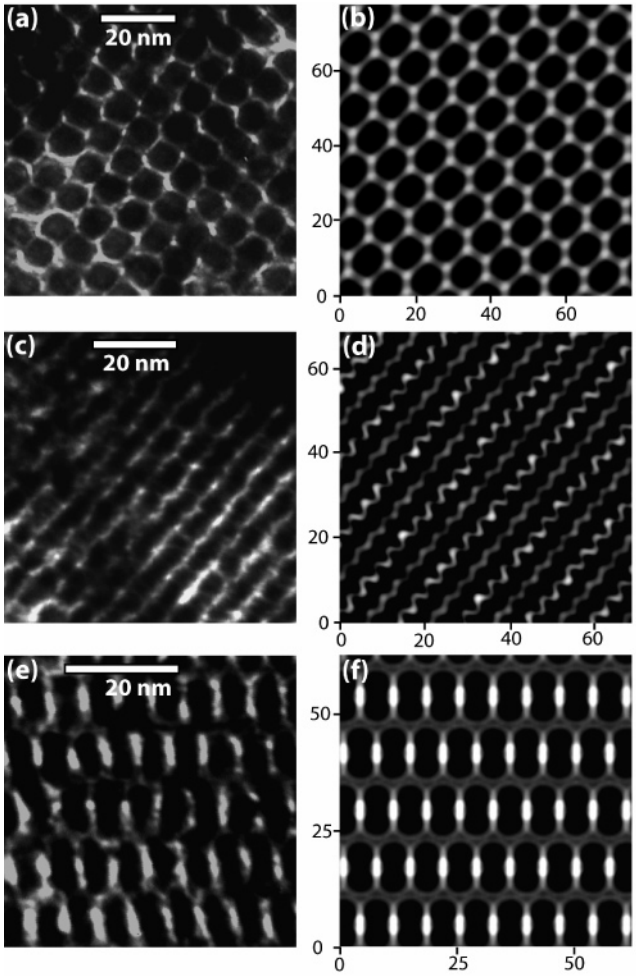

Figure 7. Transmission electron micrographs of platinum nanowire film after the removal of silica. These structures were scraped from the substrate, imaged by TEM, and compared to simulated TEM images. (a, b) Observed and simulated images along the [110] direction; (c, d) [211] and (e, f) [311] projections.

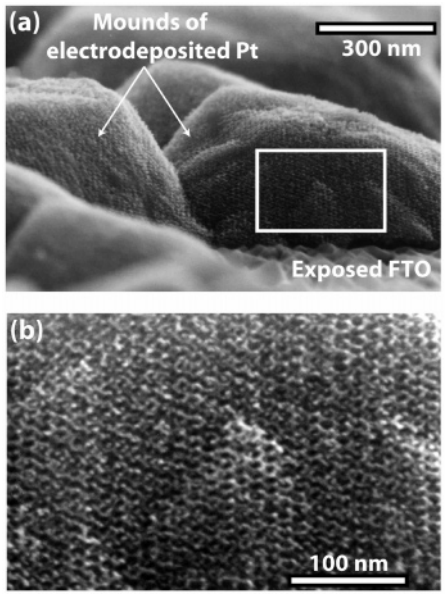

Figure 8. FESEM images of platinum replicas. (a) Top-view for a platinum replica film after the silica has been etched using HF. The image shows mounds of platinum on the micron length scale. (b) Higher-resolution view of the region in part a highlighted with a rectangle. A 3D network structure composed of rods of platinum connected in a 3-fold manner is seen, which is a clear signature the wires were templated by the double-gyroid pore system.

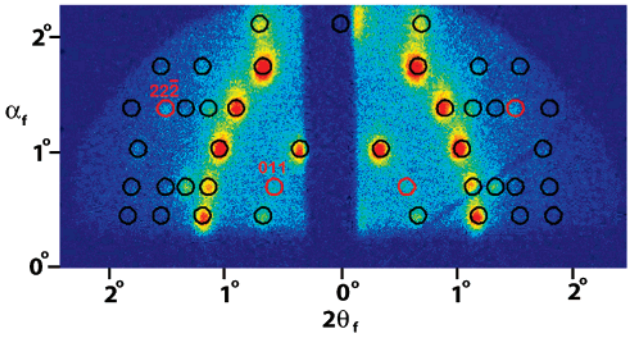

Figure 9. Observed GISAXS pattern of the platinum film after silica removal. The circles indicate the simulated peak positions. The film is contracted slightly further relative to the nanoporous silica film. A few additional peaks appear that are due to additional symmetry breaking and are shown in red.

films as they become less ordered and less oriented (as the redox couple is able to move through defects and irregular mesopore connections). However, this type of accessibility is qualitatively different from the double-gyroid films reported here, for which the substrate accessibility is determined by the regular mesopore structure. It needs to be emphasized here that nanoporous films assembled from spherical micelles of other surfactants may be accessible. The accessibility in micellar cubic systems ($Fm\bar{3}m$ or $Im\bar{3}m$ derived) will depend on the extent of overlap between adjacent pores. In the double-gyroid system, accessibility is guaranteed because of the unique bicontinuous nature of its pore system.

3.4. Nanofabrication of Inverse Double-Gyroid Platinum Films. There have been previous reports of electrochemical deposition within nanoporous silica films.[17,55−59] However, these were either in contracted 2D hexagonal films[55,57,58] with pores parallel to the substrate (meaning the deposition occurred through film defects, regions of nanostructure disorder, or microporosity) or in cagelike cubic structures with irregular pore openings. As a result, none of these electrodeposited structures retain good order after silica removal by etching. Here, we report the first electrochemical deposition of metals into a true double-gyroid-based nanoporous silica film. The metal fills each of the two continuous pore systems, and because of the 3D nature of the pore system and the high pore filling, the nanowire structures are stable after removal of the silica and retain the local and long-range order imposed by the nanopore system of the original film. TEM and FESEM micrographs of a platinum nanowire film after removal of the silica by etching in

(55) Wang, D. H.; Zhou, W. L.; McCaughy, B. F.; Hampsey, J. E.; Ji, X. L.; Jiang, Y. B.; Xu, H. F.; Tang, J. K.; Schmehl, R. H.; O'Connor, C.; Brinker, C. J.; Lu, Y. F. *Adv. Mater.* **2003**, *15* (2), 130−133.
(56) Wang, D. H.; Luo, H. M.; Kou, R.; Gil, M. P.; Xiao, S. G.; Golub, V. O.; Yang, Z. Z.; Brinker, C. J.; Lu, Y. F. *Angew. Chem., Int. Ed.* **2004**, *43* (45), 6169−6173.
(57) Gu, J. L.; Shi, J. L.; Chen, H. R.; Xiong, L. M.; Shen, W. H.; Ruan, M. L. *Chem. Lett.* **2004**, *33* (7), 828−829.
(58) Luo, H. M.; Wang, D. H.; He, J. B.; Lu, Y. F. *J. Phys. Chem. B* **2005**, *109* (5), 1919−1922.
(59) Wang, D. H.; Kou, R.; Gil, M. P.; Jakobson, H. P.; Tang, J.; Yu, D. H.; Lu, Y. F. *J. Nanosci. Nanotechnol.* **2005**, *5* (11), 1904−1909.

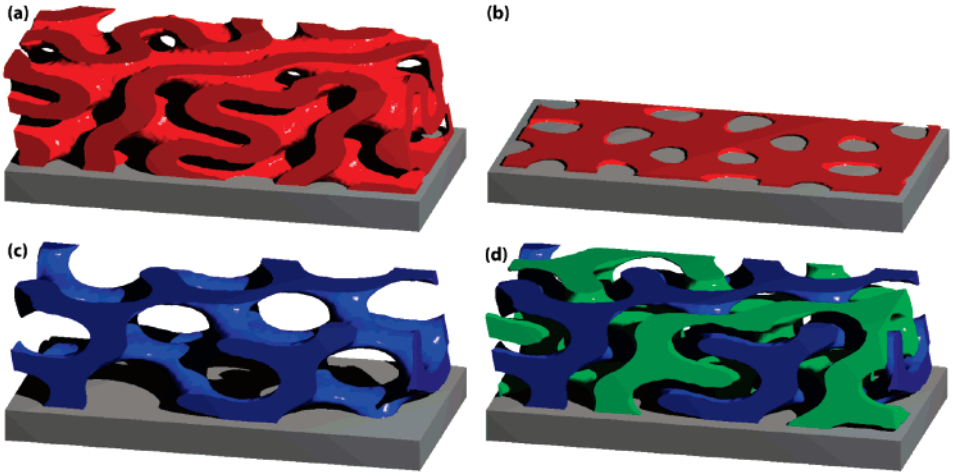

Figure 10. Three-dimensional rendering of the (211) oriented contracted double-gyroid films reconstructed from GISAXS, TEM, and FESEM data. (a) Nanoporous silica film with approximately 3 nm thick walls. (b) Footprint of the substrate exposed to solution for electrochemical experiments. (c) One pore network in blue; (d) both non-interesting pore networks (blue and green). The fabricated nanowire networks have the structure shown in part d with approximately 3 nm diameter wires.

hydrofluoric acid are shown in Figures 7 and 8, respectively. The presence of mounds of Pt on FTO substrate (as opposed a Pt film with uniform thickness) indicates that Pt is electrodeposited faster at some locations than other. However, we have also electrodeposited Pt on bare FTO substrates using identical deposition procedures, and the morphology of the deposits at the micrometer level is the same on bare FTO as it is on double-gyroid-coated FTO. Further optimization of synthesis parameters (such as the use of pulsed electrodeposition technique) may be required to attain uniform thickness deposits; efforts are currently underway in that direction. The TEM simulations that best fit the observed TEM images were obtained as discussed above with a contour level equal to 0.5, except they were based on a structure where platinum fills the both pore systems and the original silica wall is absent. The observed TEM images compare very well with the simulated electron density projections for the [111], [211], and [311] directions.

GISAXS patterns were also collected from the Pt films after silica removal (Figure 9) and show a spot pattern consistent with a double-gyroid structure, indicating that long-range order and orientation of the structure is retained in Pt deposits as well. The observed GISAXS spot pattern and relative intensities closely match that for the nanoporous silica film (as would be expected by the Babinet Principle). This also shows that the two continuous nanowire systems do not shift significantly relative to one another in contrast to that observed in carbon materials templated by MCM-48.[60] GISAXS simulations show that if this were the case, the relative intensity of the (110) family would increase dramatically, whereas the (211) family would be strongly suppressed. The fact that the nanowire networks do not shift may be due to the fact that they are independently (and regularly) connected to the substrate or perhaps due to the presence of interconnections.

The contour of the G level surface that best simulated the nanoporous silica TEM images was 1.1 (corresponding to a silica wall thickness of ~5 nm at 24d Wyckoff position prior to applying the rotation matrices and contraction), whereas the contour that best simulated the platinum replica TEM images was 0.5 (corresponding to a spacing of ~2.1 nm between two Pt nanowire networks at the 24d Wyckoff position before applying the rotation matrices and contraction). Thus, the spacing between the two enantiomeric networks of Pt is less than the silica wall thickness, and it appears that Pt networks penetrate into the silica wall to a significant extent. This penetration can be explained by the existence of microporosity in the silica wall. For 2D hexagonal silica powders templated by EO−PO−EO surfactants, EO is often occluded in the silica wall, giving rise to a microporous corona around the pore.[61,62] Neglecting the effects of multiple scattering and focusing may lead to some discrepancies between the actual silica wall thickness and that calculated from the model; however, the unexpectedly large thickness of Pt networks may also be explained by the presence of microporosity in the silica wall. Pt can get electrodeposited in the micropores present in the silica wall in addition to the mesopores, and thus the effective thickness of Pt nanowire networks will be larger than the pore size in the original silica template. This will mean that the two networks are closer to each other than the width of the silica wall. After the contraction is applied, both silica wall thickness and pore size are reduced to ~3 nm. Without modeling the details of the microporosity, we represent the nanostructure using an intermediate contour value of 0.8. A 3D reconstruction of the oriented and contracted double gyroid films with this contour is shown in Figure 10.

The volume void fraction and mesopore surface area were calculated numerically from the 3D reconstruction of the film to be 0.46 cm^3_{pore}/cm^3_{film} and 5.4×10^6 $cm^2_{surface}/cm^3_{film}$. Also, the critical angle for X-ray scattering from the calcined nanoporous silica film was measured by GISAXS to be 0.165°. The average electron density of the calcined film is

(60) Kaneda, M.; Tsubakiyama, T.; Carlsson, A.; Sakamoto, Y.; Ohsuna, T.; Terasaki, O.; Joo, S. H.; Ryoo, R. *J. Phys. Chem. B* **2002**, *106* (6), 1256−1266.

(61) Imperor-Clerc, M.; Davidson, P.; Davidson, A. *J. Am. Chem. Soc.* **2000**, *122* (48), 11925−11933.

(62) Ryoo, R.; Ko, C. H.; Kruk, M.; Antochshuk, V.; Jaroniec, M. *J. Phys. Chem. B* **2000**, *104* (48), 11465−11471.

then calculated from the critical angle to be 348 electrons/nm^3. The density of the silica wall calculated from the average film electron density and void fraction is 2.13 g/cm^3. This yields an internal mesopore surface area of the contracted film of 468 m^2/g. For comparison, a 2D hexagonal silica phase with similar wall thickness and pore diameter has an internal mesopore surface area of 80 m^2/g. Also, from this structural model, the footprint in contact with the electrode can be modeled. The planar void fraction of slices parallel to the electrode, parallel to the (211) planes, of the double-gyroid nanoporous silica film range from 0.29 to 0.61 depending on the height of the slice. The slice with the highest silica density (lowest void fraction) should be the most favored on the hydrophilic substrates used here. Hence, we expect the exposed fraction of the substrate area to be close to the lower value in this range (0.29). The experimentally determined fractional exposed area (0.31) is indeed close to the expected value. The footprint left by this slice is shown in Figure 10b. FTO has a surface roughness on a length scale slightly larger than the lattice parameters of the double-gyroid structure. For ease of viewing and clarity, we have shown the FTO surface to be flat in the illustrations.

This synthesis method of controlling curvature by controlling the size of the silica clusters in the coating solution is expected to be generalizable to non-silica systems as well. This may pave the way for the synthesis of other technologically important metal oxides such as TiO_2 and SnO_2. The electrodeposition method used above to fabricate platinum nanostructures using nanoporous double-gyroid silica as a template has been replicated with several metals and semiconductors such as cobalt, cadmium selenide, and cadmium telluride. The details of the electrodeposition route to synthesize ordered nanostructured semiconductors using double-gyroid silica as template will be reported elsewhere.

4. Conclusions

Nanoporous silica films having the double-gyroid structure have been synthesized using a synthesis strategy that relies on controlling the curvature at the silica−surfactant interface by controlling the aging of the coating solution prior to EISA. High-quality double-gyroid silica films can be prepared over a very broad range of synthesis conditions such as the silica to template ratio, aging time, and relative humidity during dip-coating. Using electrochemical impedance spectroscopy, we have been able to quantitatively estimate the area of the substrate accessible through the pore system. Double-gyroid silica films show a much higher accessible substrate area (31% of the area covered by the nanoporous film is accessible) than other commonly synthesized nanostructures such as centered rectangular *c*2*mm* or rhombohedral $R\bar{3}m$. Using small-angle X-ray scattering and FESEM imaging, the structure of the films has been established. The films have a very open and accessible pore system with approximately 3 nm thick silica walls and 3 nm wide pores. The highly open nature of the pore systems allows one to electrodeposit several metals and semiconductors in them to create a three-dimensionally interconnected "network-of-rods" structure characteristic of the inverse double-gyroid phase. The ability to synthesize thin films of ordered nanostructured semiconductors with wall thickness smaller than 5 nm opens up opportunities to study the interesting quantum confinement effects seen in these semiconductors and potentially fabricate high-efficiency photovoltaic and thermoelectric devices from them.

Acknowledgment. The authors acknowledge financial support from the National Science Foundation under the CAREER Award (0134255-CTS); the use of the NSF funded facility for In situ X-ray Scattering from Nanomaterials and Catalysts (MRI Program Award 0321118-CTS); and the use of the advanced photon source supported by the U.S. Department of Energy, Office of Science, Office of Basic Energy Sciences, under Contract W-31-109-ENG-38. Also, we thank Dr. Sudhakar Balijepalli (SBalijepalli@dow.com) of Dow Chemical Company for providing the $EO_{17}-PO_{12}-C_{14}$ copolymer.

CM062136N